Near-wall Hindered Diffusion in Convective Systems: Transport Limitations in Colloidal and Nanoparticulate Systems

Stanislav V. Sokolov, Enno Kätelhön, and Richard G. Compton*

Department of Chemistry, Physical and Theoretical Chemistry Laboratory, South Parks Road, Oxford University, Oxford OX1 3QZ, United Kingdom

E-mail: richard.compton@chem.ox.ac.uk

Phone: +44 (0) 1865 275957. Fax: +44 (0) 1865 275410

*To whom correspondence should be addressed

Abstract

Redox flow cells have a significant potential as efficient, scalable energy storage and use of nano-materials is likely to increase the energy density even further. Efficient cell design requires understanding of mass transport effects and for colloidal systems the theoretical assumptions commonly used for molecular species require re-evaluation. In the present work the effect of near-wall hindered diffusion is investigated in the convective-diffusive system of a colloidal suspension of nanoparticles. The rotating disk electrode system is used as a model due to wide applicability of the technique for the battery testing. A major influence of near-wall hindered diffusion is observed in the resulting concentration profiles of the nanoparticles (aqueous concentration as a function of distance) and the current responses in the case of the colloidal suspensions, and the finding is likely to have a significant impact on the understanding of physical processes underlying the practical cell design and modelling.

Introduction

Efficient, scalable and low-cost energy storage remains a limiting factor to a wide adoption of renewable energy sources and a range of potential solutions have been developed over the years.[1,2] Electrochemical methods provide an attractive option due to relative simplicity, potential scalability and low cost.[3] Redox flow batteries meet many of the required criteria due to decoupled power/energy-storage design. One of the main limitations of traditional redox flow systems is poor energy density due to low ion concentrations used and limited cell-voltage. Nanoparticles have significant potential to alter the field of energy production and storage. A novel approach involves use of colloidal suspension of electroactive nanoparticles as a "nanoelectrofuel" where the charge and discharge rates are enhanced due to the presence of nanoparticles, while the resultant increase in viscosity is negligible.[4,5] Efficient practical applications and further improvements in the efficiency require understanding of physical processes which arise in such colloidal nanoparticulate systems. One of the main ap-

proaches to modelling convective-diffusive systems has been the Colloidal Filtration Theory (CFT) originally introduced by *Yao et.al*[6] which takes into account near-wall hydrodynamic effects and interactions of molecular and solute nature as described by Derjaguin Landau Verwey Overbeek (DLVO) theory.[7] The CFT has been successfully applied to diverse systems ranging from colloidal suspensions[8] to movement of bacteria in a contaminated sandy aquifer.[9] Earlier models neglected hydrodynamic retardation of diffusion[10] and as a result were not accurate for smaller colloids ($r < 100$ nm). Current CFT approaches take into account the hydrodynamic effects and demonstrate high degree of accuracy.[11–14] These models feature high degrees of complexity and in many cases require numerical simulations. The aim of the present work is to provide a treatment of a convectional-diffusional system from electrochemical point of view with the main aim of predicting the current response rather than the collector properties.

The rotating disk electrode (RDE) has proved to be an invaluable tool[15,16] for the study of electrochemical processes as evidenced by the large body of literature. RDE technique has been successfully used to elucidate reaction mechanisms[17] and finds a wide variety of industrial applications (in particular battery testing)[18–20] and was successfully applied to characterize electrochemical behaviour of colloidal suspension of nanoparticles.[21–23] Advantages of the rotating disk are: the bulk solution is well-mixed and homogeneous, the rotation rate allows control of the hydrodynamic layer thickness, and most importantly the steady-state current response allows accurate analysis of the systems and extraction of kinetic parameters. In addition the RDE electrode involves an electrode of macro-dimensions and the resulting high current signal does not require the setup to be shielded by a Faraday cage, unlike the microelectrodes which often suffer from interferences due to the low current signal.

Traditionally the focus of RDE studies has been on molecular electrochemistry and only recently has the focus shifted to colloidal systems. Unlike molecular systems, colloidal suspensions introduce additional complications to the analysis and theoretical treatment due

to non-uniform diffusion coefficient of the species as a result of the hindered diffusion near surfaces. As the particles approach a solid boundary they experience hydrodynamic retardation and as a result the diffusion coefficient is lowered, which leads to a reduction in the observed mass transport. In the following work we present a theoretical treatment of a colloidal nano-particulate system undergoing electrolysis at a RDE and contrast it with the behaviour of a traditional molecular system. In particular we demonstrate the following physical insights: near-wall hindered diffusion plays a dominant role for mass transport in convective systems and the balance of electron tunneling and near-wall hindered diffusion leads to a significant change in the position of electron tunnelling compared to molecular systems. We combine mass transport of the particles and kinetics of the electron transfer with an inclusion of the electron tunneling in order to predict the current response of the electrochemical convective-diffusive system.

Theory

In this section we initially consider the hydrodynamics of the rotating disk and the convective-diffusive mass transport taking place. We then consider the cases of uniform and near-wall hindered diffusion and develop a model which incorporates electron tunnelling into Butler-Volmer kinetics demonstrating the impact of these considerations on the diffusion limited current at a rotating disk. We consider the case of high ionic strength, which is typical for almost all batteries, which leads to negligible double layer effects in accordance with the DLVO theory and corresponding simplifications of the model. As a result the conditions are favorable to deposition of the particles and there is no energy barrier. In addition the nanoparticles arriving at the electrode held at a high overpotential are dissolved electrolytically and as a result there is no perturbation to the resultant concentration profile of the particles at the electrode surface.

Hydrodynamics of a rotating disk

The velocity profile at the rotating disk is based on the solution of the Navier-Stokes equations as provided analytically by Von Kaŕmań[24] and numerically by Cochran.[25] The complete hydrodynamics description of the rotating disk involves for simplicity three dimensionless components: radial, azimuthal and the axial velocities. According to this solution at the disk surface there exists a relatively stagnant solution layer. This layer is known as hydrodynamic layer and its thickness is defined in accordance with Equation 1, where δ_0 is the hydrodynamic layer thickness, υ is the kinematic viscosity, ω is the angular velocity (defined in accordance with Equation 2) and f is the frequency.

$$\delta_0 = 3.6\sqrt{\frac{\upsilon}{\omega}} \tag{1}$$

$$\omega = 2\pi f \tag{2}$$

Within the hydrodynamic layer, the radial flow contribution is negligible and only axial velocity needs to be taken into account. The radial and azimuthal velocities do not perturb the electrochemical response of the system and only axial velocity is of significant importance. The axial velocity v_x is a function of separation distance x from the rotating electrode and for electrolytes, assuming a high Schmidt number (defined as the ratio of momentum diffusivity (viscosity) and mass diffusivity),[26] is given according by Equations 3-4[24]

$$v_x = \sqrt{\upsilon\omega}\left(\frac{-0.51\omega x^2}{\upsilon} + \frac{\omega^{3/2}x^3}{3\upsilon^{3/2}} - ...\right)\ for\ x < \delta_0 \tag{3}$$

$$v_x = -0.886\sqrt{\upsilon\omega}\ for\ x > \delta_0 \tag{4}$$

which show that the axial velocity decreases to zero at the electrode surface and as a result within close proximity to the electrode the mass transport will be dominated by the diffusion process rather than convection. An infinitely large rotating disk is uniformly accessible[27] and as result the velocity profile is independent of the radial component and hence only

the knowledge of axial velocity is required for the resolution of the mass transport problem which effectively simplifies the equations to one dimension.

The landmark theoretical treatment for the flux of electroactive species to the rotating disk was given by V. Levich,[28,29] who solved the diffusion-convection equation (Equation 5) under steady state conditions (Equation 6), where $\frac{\partial c}{\partial t}$ is change of concentration with time, $\frac{\partial^2 c}{\partial x^2}$ is a diffusion term, and $v_x \frac{\partial c}{\partial x}$ denotes the convection term.

$$\frac{\partial c}{\partial t} = D\frac{\partial^2 c}{\partial x^2} - v_x \frac{\partial c}{\partial x} \tag{5}$$

$$D\frac{d^2 c}{dx^2} - v_x \frac{dc}{dx} = 0 \tag{6}$$

Levich developed the insight that the rotating disk is uniformly accessible (a property only possessed by a select few hydrodynamic systems[27] but including the wall-tube electrode) and derived the concentration profile of the reactants under first order-convection approximation given by Equation 7.

$$c(x) = \frac{\gamma\left(\frac{1}{3}, \frac{0.51\omega^{3/2}x^3}{3Dv^{1/2}}\right)}{\Gamma\left(\frac{1}{3}\right)} c^* \tag{7}$$

where Γ and γ are the full and incomplete Gamma functions respectively. The steady state limiting current is given by Equation 8.

$$I_{ss} = 0.62FAc^* D^{2/3}\omega^{1/2}v^{-1/6} \tag{8}$$

where F is the Faraday constant, A is the electrode area, c^* is the bulk concentration, and D is the bulk diffusion coefficient of the species. This equation provides a useful comparison for the simulated system and allows validation of the numerical simulations in the absence of the near-wall hindrance.

Levich assumed that the diffusion coefficient is independent of x, an assumption which is usually exact for molecular species, but can potentially introduce inaccuracy in the case

of nanoparticles, which are larger in size.[30–32] It has been demonstrated by Brenner[33] that a moving particle near a wall experiences a hindrance due to a hydrodynamic force. The effect is known as near-wall hindered diffusion and is significant for colloidal systems as demonstrated with a wide range of experimental techniques.[30,32,34–36] The effect manifests itself in the apparent reduction of the diffusion coefficient within close proximity to the solid boundary. As a result a distance dependent correction factor λ is required. In the present work we extend the Levich's analysis of the rotating disk to a colloidal system. We consider a system of electroactive particles and solve the diffusion-convection equation for species of various sizes accounting for the near-wall hindrance term. For the solution of the mass transport to a rotating disk we use the analysis developed by Elimelech.[37] The mass transport problem can be formulated mathematically by Equation 9,

$$\frac{\partial c}{\partial t} = \frac{\partial}{\partial x'}(\lambda(x')D\frac{\partial c}{\partial x'}) - v_{x'}\frac{\partial c}{\partial x'} = 0 \tag{9}$$

$$x' = x - r \tag{10}$$

where c is the concentration of electroactive species, x' is the separation between the nanoparticle edge and the electrode and r is the radius of a particle. In order to facilitate ease of analysis and reduce complexity of the analysis the equation is solved under steady-state condition.

Near-wall hindered diffusion

As a particle approaches a solid boundary it experiences reduced mobility and a result the diffusion coefficient is no longer uniform and a correction factor is needed. The detailed analysis has been provided by Brenner[33] and the solution was given in terms of an infinite series. An approximation was introduced by Bevan and Prieve[38] in order to facilitate ease

of use and this expression has been used in the present work as shown in Equation 11.

$$\lambda = \frac{6x,^2 + 2rx,}{6x,^2 + 9rx, + 2r^2} \tag{11}$$

The resultant diffusion coefficients of the particles will depend on their position with respect to a boundary as shown in Equation 14.

$$D_{x,} = D_{bulk}\lambda(x,) \tag{12}$$

where D_x is the diffusion coefficient at a given distance from the electrode, and D_{bulk} is the bulk diffusion coefficient. For an RDE system which involves a planar electrode the most important parameter is electrode/particle separation, as a result unlike the case described by *Eral et al.*[12] the angular component will be insignificant as it will not have an effect on the observed current response and the main contribution will be the normal component of the diffusion.

Justification of applicability of near-wall hindered diffusion

The derivation obtained by Brenner[33] is only strictly valid for unperturbed system and hence application to the RDE requires justification. According to the solution for the velocities provided by Von Karman[24] and Cochrane[25] at the surface the azimuthal component is equal to unity, and both axial and radial components decay to zero. As a result provided that the flow to the disk is laminar a virtually stagnant layer is observed, which allows us to make use of the Brenner analysis. At very fast rotation rates (high Reynolds numbers, $Re = \frac{\omega r^2}{v} > 2000$) the flow will become turbulent and as a result the treatment presented in the present work would no longer be applicable. An additional important point is the centrifugal force experienced by a particle with effective mass m^* (defined in accordance with

Equation 13) at the close proximity to the electrode.

$$m^* = \frac{4}{3}\pi r_{np}^3(\rho_{np} - \rho_{solvent}) \tag{13}$$

$$v_{np} = \frac{m^*\omega^2 r}{6\pi\mu r_{np}} \tag{14}$$

where m^* is the effective mass, ρ is the respective densities of a particle and a solvent, v_{np} is the radial velocity of the particle, μ is the dynamic viscosity. The resultant radial velocity even for the large nanoparticles, $r \approx 50\ nm$, is small and does not lead to significant perturbations and as result near-wall hindrance to diffusion remains applicable as the dominant mass transport. Note also for such small particles their radius is tiny compared to the thickness of the hydrodynamic layer so that the mass transport enhancement seen for much larger particles is not significant.[39–42]

Unlike traditional electrochemical simulations for the case of hindered diffusion an alternative electrical flux measurement is required as the diffusion coefficient at the electrode surface is zero, which leads to an apparent zero mass flux (f) for the simulation.

$$f = D_{x=0}\frac{dc}{dx}\bigg|_{x=0} = 0 \tag{15}$$

if the concentration gradient at the electrode is measured in accordance with Equation 15, as is usual in many past simulations.[43–46] On the other hand if the electrical flux is measured at a small distance from the electrode where the diffusion coefficient is not zero, the electrical flux will change with the spatial variation of the diffusion coefficient. As a result an alternative approach is warranted in order to simulate the actual electrical flux of the species.

In reality the electron transfer takes within a zone close to the electrode surface where electron tunnelling is possible[47,48] and as a result a more complex boundary condition is warranted for the solution of convection diffusion equation.

Electron tunnelling

In order to measure the simulated electrical flux and avoid the problems highlighted in the previous section, it is possible to incorporate electron tunnelling which is confined to a certain volume in close proximity to the electrode surface.[47–50] Electron tunnelling is a distant dependent problem and its probability P is thought to fall off approximately exponentially with increasing distance in accordance with Equation 16:

$$P = ve^{-\beta x} \tag{16}$$

where v is a frequency factor (s^{-1}), and β is the electron-tunnelling decay factor (m^{-1}) is dependent on the medium where the electron transfer takes place and for aqueous solvent is equal to 1.59 $\mathring{A}^{-1}$.[46,51,52]

Butler-Volmer Kinetics

The rate of electron transfer can be modelled at every point in the solution in accordance with the Butler-Volmer kinetics equation,[46,53] which describes the rate of electron transfer dependence on the potential applied. For a single electron transfer reaction, for a redox couple where both A and B have the same diffusion coefficient the Butler-Volmer concentration dependence is defined in accordance with Equation 21.

$$B \rightleftharpoons A + e^{-} \tag{17}$$

$$D_A = D_B \tag{18}$$

$$[B] = [A]_{bulk} - [A] \tag{19}$$

$$f_{BV} = ([A](x)e^{-\alpha\eta} + ([A](x) - [A]_{bulk})e^{(1-\alpha)\eta}) \tag{20}$$

$$\eta = \frac{F}{RT}(E - E_f^0) \tag{21}$$

where $[j]_a$ is the bulk concentration, $[j]$ is the concentration of a given species, α is the charge transfer coefficient (for many reactions $\alpha \approx 0.5$),[54,55] k_0 is the standard heterogeneous rate constant and η is the dimensionless potential with respect to the formal potential, E_f, for a given species couple, F is the Faraday constant, R is the gas constant and T is the temperature. In the absence of tunnelling the electrical flux is given in accordance with the ideal Butler-Volmer equation (Equation 22):

$$f = k_0 f_{BV} \tag{22}$$

Dimensionless Parameters

In order to simplify subsequent analysis dimensionless parameters will be used. Conventional dimensionless parameters were chosen in order to combine the angular velocity and the diffusion coefficient of the particles. This allows considerable simplification of convection-diffusion equations.[15,45]Equations (ODEs) were converted to a dimensionless form using the parameters described in Table 1.

Table 1: Dimensionless parameters used for the simulation

Dimensional Parameter	Dimensionless Form
Velocity constant L	$L = (0.51023(2\pi f)^{3/2}\upsilon^{-1/2}$
Time t	$T = (L^2 D_{bulk})^{1/3} t$
Space x	$W = (\frac{L}{D_{bulk}})^{1/3} x$
Concentration c	$C = \frac{c}{c_{bulk}}$
Tunnelling Constant β	$\beta^* = (\frac{L}{D_{bulk}})^{-1/3}\beta$
Radius of a particle r	$R = (\frac{L}{D_{bulk}})^{1/3} r$
Frequency factor v	$v^* = (\frac{L}{D_{bulk}})^{1/3} v$
Heterogeneous rate constant k_0	$K = \frac{(\frac{L}{D_{bulk}})^{-1/3} k_0}{D_{bulk}}$
Butler-Volmer f_{bv}	$F_{BV} = (Ce^{-\alpha\eta} + (C-1))e^{(1-\alpha)\eta}$

The relationship between dimensional and dimensionless values used in the simulations is given in Table 2:

Table 2: Conversion between dimensional and dimensionless parameters

	Dimensional Value	Dimensionless Value at 10 Hz		Dimensionless Value at 50 Hz	
Parameter		$r_{np} = 1\ nm$	$r_{np} = 50\ nm$	$r_{np} = 1\ nm$	$r_{np} = 50\ nm$
β	$1.57 \times 10^{10} m^{-1}$	1.6×10^5	0.45×10^5	0.7×10^5	0.19×10^5
v	$0.001 - 1\ s^{-1}$	$6.3 \times 10^6 - 2.3 \times 10^7$	$6.3 \times 10^9 - 2.3 \times 10^{10}$	$1.2 \times 10^6 - 4.6 \times 10^6$	$6.3 \times 10^9 - 2.3 \times 10^{10}$
$E - E_f$	0.25 to -0.38 V	10 to -15	10 to -15	10 to -15	10 to -15

Extension of Butler-Volmer Kinetics applied to the RDE

Levich solved the Equation 6 under the conditions of infinite kinetics (in accordance with the boundary condition $c_{x=0} = 0$). It is possible to extend the solution by assuming that the surface concentration of species is controlled by Butler-Volmer kinetics. Hence the following Equation 24 must be solved:

$$D\frac{d^2c}{dx^2} - v_x\frac{dc}{dx} = 0 \tag{23}$$

subject to the boundary conditions at the electrode surface and in the bulk:

$$D\frac{dc}{dx}\Big|_{x=0} = k_0 f_{BV} \;\; and \;\; c_{x=\infty} = c_{bulk} \tag{24}$$

The analytical solution for the concentration profile with the finite Butler-Volmer kinetics was obtained using Mathematica Software (Wolfram Research, Inc., Mathematica, Version 10.3, Champaign, IL (2016).) and is given in accordance with Equation 25 in dimensionless form:

$$C(W) = \frac{3e^{\alpha\eta} + \sqrt[3]{3}K\Gamma\left(\frac{1}{3}\right)e^{\alpha\eta} - \sqrt[3]{3}K\gamma\left(\frac{1}{3},\frac{W^3}{3}\right) + \sqrt[3]{3}K\Gamma\left(\frac{1}{3}\right)}{3e^{\alpha\eta} + \sqrt[3]{3}K\Gamma\left(\frac{1}{3}\right)e^{\alpha\eta} + \sqrt[3]{3}K\Gamma\left(\frac{1}{3}\right)} \tag{25}$$

where K is the dimensionless heterogeneous rate constant. At highly negative overpotentials the expression becomes equivalent to the Levich concentration profile which is consistent with the assumptions of zero concentration at the electrode surface used by Levich, while at high positive overpotentials the concentration is uniform as no depletion of the reactants takes place.

$$\lim_{\eta\to-\infty} C(W) \to 1 - \frac{\gamma\left(\frac{1}{3},\frac{W^3}{3}\right)}{\Gamma\left(\frac{1}{3}\right)} \tag{26}$$

$$\lim_{\eta\to\infty} C(W) \to 1 \tag{27}$$

By evaluating the derivative of Equation 25 at the electrode surface the electrical flux response can be evaluated in accordance with Equation 28.

$$F = \frac{3K}{3e^{\alpha\eta} + \sqrt[3]{3}K\Gamma\left(\frac{1}{3}\right)e^{2\alpha\eta} + \sqrt[3]{3}K\Gamma\left(\frac{1}{3}\right)} \tag{28}$$

where F is the dimensionless electrical flux.

Combining tunnelling and the convection-diffusion equations

The concentration profile will be time dependent, however in the present work we consider the steady-state case.[47,56] At steady state the concentration profile does not change with

time and we can equate the tunnelling terms and convection-diffusion equations in order to yield the Equation 29 in the case of isotropic diffusion coefficient and Equation 30 for the near-wall hindered diffusion, which is required to be solved in order to obtain the steady-state concentration profile ($\frac{\partial[A]}{\partial t} = 0$) and calculate the resulting electrical flux.

$$0 = \frac{\partial[A]}{\partial t} = \frac{\partial}{\partial x}(D\frac{\partial[A]}{\partial x}) - v_x\frac{\partial[A]}{\partial x} - \upsilon e^{-\beta x} f_{BV}(x) \tag{29}$$

$$0 = \frac{\partial[A]}{\partial t} = \frac{\partial}{\partial x'}(\lambda(x')D\frac{\partial[A]}{\partial x'}) - v_x'\frac{\partial[A]}{\partial x'} - \upsilon e^{-\beta x'} f_{BV}(x) \tag{30}$$

subject to the boundary condition, where f_{BV} is the function of x:

$$\left.\frac{dc}{dx}\right|_{x=0} = \left.\frac{dc}{dx'}\right|_{x'=0} = 0 \tag{31}$$

The dimensionless form of Equations 29-30 is given below:

$$\frac{dC}{dT} = \frac{d^2C}{\partial W^2} + W^2\frac{dC}{dW} - \upsilon^* e^{-\beta^* W} F_{BV}(W) = 0 \tag{32}$$

$$\frac{d^2C}{dW^2} + (\frac{dln(\lambda(W))}{dW}(\lambda(W) + \frac{W^2}{\lambda(W)})\frac{dC}{dW} - \frac{\upsilon^* e^{-\beta^* W}}{\lambda(W)} F_{BV}(W) = 0 \tag{33}$$

They were solved subject to the boundary condition:

$$\left.\frac{\partial C}{\partial W}\right|_{W=0} = 0 \tag{34}$$

Flux and current output

The electron transfer can take place at any point in the solution with the probability given with Equation 16, and as a result the overall electrical flux will correspond to the sum of all flux contributions at every spatial point as defined in accordance with Equation 38. The current I is proportional to the area of the electrode and is given in accordance with Equation

35.

$$I = FAc^{*}v \int_{0}^{\infty} e^{-\beta x} f_{BV}(x)\, dx \tag{35}$$

Full model of the system

By combining knowledge of the mass transport of nanoparticles which involves convection and diffusion and the kinetics of heterogeneous electron transfer which takes place once the particles are in close proximity to the electrode (accounted by the standard Butler-Volmer model and electron tunnelling) it is possible to derive the resultant current response of the system and predict the behaviour of the colloidal suspension, which will depend on the above components. The electron tunnelling was included to allow realistic modelling of the electron transfer taking place and to avoid the apparent zero flux caused by the reduction of the diffusion coefficient at the electrode. The model is represented schematically in Figure 1 which shows the rotating disk electrode and the theoretical parts of the model. As the particles collide with the electrode surface they are electrolytically destroyed and as a result do not perturb the local concentration at the electrode.

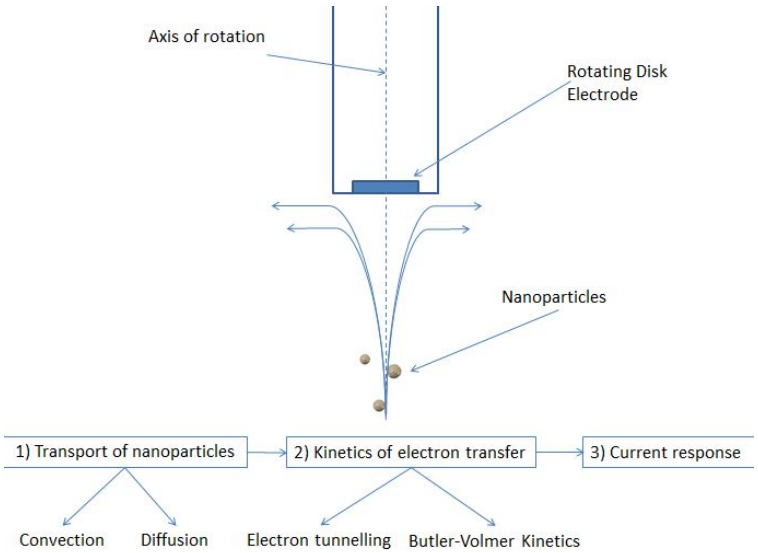

Figure 1: Schematic representation of the rotating disk system and the components of the theoretical model, which include mass transport of the particles, kinetic model of the electron transfer and the overall current response

Simulation

Discretization and Numerical Algorithm

The Equations 32-33 were discretized, solved and plotted using Mathematica software (Wolfram Research, Inc., Mathematica, Version 10.2, Champaign, IL (2015)). The explicit Runge-Kutta method was trialled initially, but showed poor stability and excessive calculation times. Hence an implicit Runge-Kutta method[57] was used for the resolution of the numerical problem with an adaptive spatial grid through the use of the built-in solver. An expanding-adaptive grid was used for discretization. Within close proximity to the electrode the grid step-size was kept to machine level of precision (2×10^{-16}) in order to ensure accuracy of representation of the exponential decay term. The algorithm uses the previous step in order to evaluate the next step size within the specified error tolerance by comparing between several orders of Runge-Kutta methods (Orders 2-8) used to estimate the local error and adjusts the step size accordingly. Figure S1 (supplementary material) shows a logarithmic plot of the step size used against the distance from the electrode, a generally high sampling density is observed in the region of close proximity to the electrode with a relatively sparse grid in the bulk.

Comparison

The numerical solution to Equation 29 was tested against the analytical solutions by Levich for the concentration profile and steady-state limiting current(Equations 7-8). For convenience the Levich expression for the concentration profile was converted to dimensionless form in order to facilitate ease of comparison in accordance with Equation 36.

$$C(W) = 1 - \frac{\gamma\left(\frac{1}{3}, \frac{W^3}{3}\right)}{\Gamma\left(\frac{1}{3}\right)} \tag{36}$$

Figure 2 shows the resulting concentration profiles obtained analytically (solid red line) and numerically with electron tunnelling at high overpotential (dashed blue line) assuming infinitesimally small particles and hence no hindered diffusion. An excellent agreement is observed between the two calculations. The difference between the two concentration profiles is only apparent in the region close to the electrode surface as shown in the inset, where in accordance with the analytical solution the concentration decreases to zero at the electrode surface, while the simulation shows a finite concentration gradient. It is a result of a difference in terms of boundary conditions used to obtain the solutions. In the case of analytical solution, infinite kinetics is assumed and as a result the concentration at the electrode surface is zero but for the case of electron tunnelling the boundary condition only requires the concentration gradient to be zero and as a result zero concentration will only be observed at infinite overpotential.

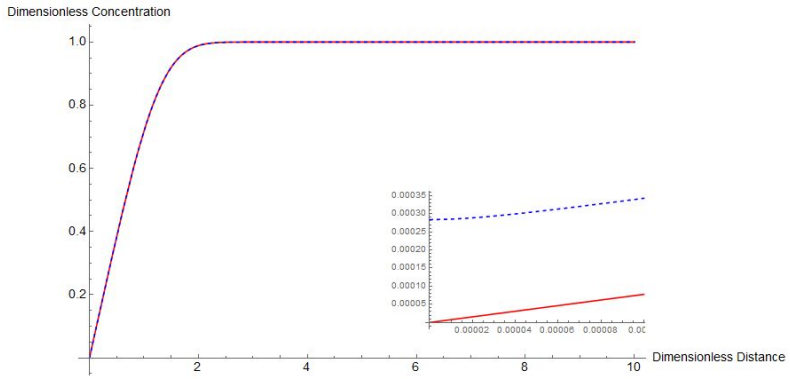

Figure 2: Comparison of the concentration profiles obtained analytically in the absence of electron tunnelling (solid red line) and numerically with electron tunnelling at high overpotential (dashed blue line). Equations 32 and 36 were used to calculate the concentration profiles

At rotation rates orresponding to the typical experimental practice ($f = 10\ Hz$), the discrepancy in the limiting steady state current between the analytical and numerical values was found not to exceed 0.07%. In addition the effects of the heterogeneous rate constant and transfer coefficients were tested through use of Tafel plots. Figure S2 (supplementary materials) shows Tafel plots of corrected current i_c against the overpotential, obtained according

to the Equation 37 for the two limiting cases, dashed red line shows the plot for highly electrochemically irreversible process with dimensionless frequency constant $v^* = 6.3 \times 10^4$ and the blue line shows a highly electrochemically reversible process with an artificially high frequency constant $v^* = 6.3 \times 10^8$. (Simulation parameters used for dimensionless conversion: $R = 1 \times 10^{-4}$, $\alpha = 0.5$, $v^* = 6.3 \times 10^4$ for irreversible case, $v^* = 6.3 \times 10^8$ for reversible case, $\beta^* = 1.57 * 10^5$ $\eta = -15$, corresponding physical values are given in Table 2)

$$\ln i_c = \ln[\frac{1}{i} - \frac{1}{i_l}] \tag{37}$$

where i_c is the corrected current, i is the measured current and i_l is the limiting current. For fast kinetics ($v^* = 6.3 \times 10^8$) the gradient of the must coincide with the Nernstian limit and be equal to 1 while for the slow kinetics the gradient is determined by the α value, which in this case is equal to 0.5. Excellent agreement is observed between the theoretical values and the simulation used in the present work.

Heterogeneous rate constant and frequency factor relationship

The relationship between "standard" Butler-Volmer kinetics and the case of electron tunnelling was tested by taking a range of β^* values and frequency factors v^* and least square fitting of the analytical Butler-Volmer result (Equation 28) to the resultant plots. Figure 3a shows an example of steady-state voltammogram obtained using the tunnelling model and the resultant fit of classic BV model (Parameters used: $\alpha = 0.5$, $v* = 10^8$, $R = 1 \times 10^{-4}$). A linear relationship was observed between the fitted K values and v^*, the gradient of each of the lines is close to β^*.

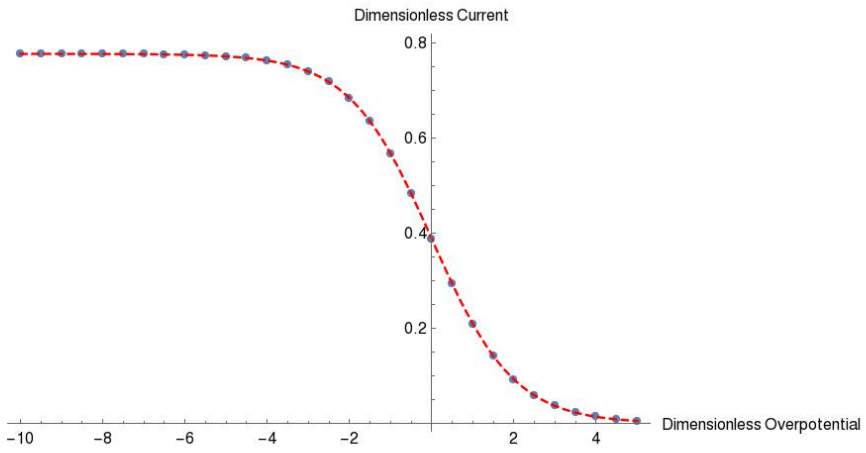

(a)

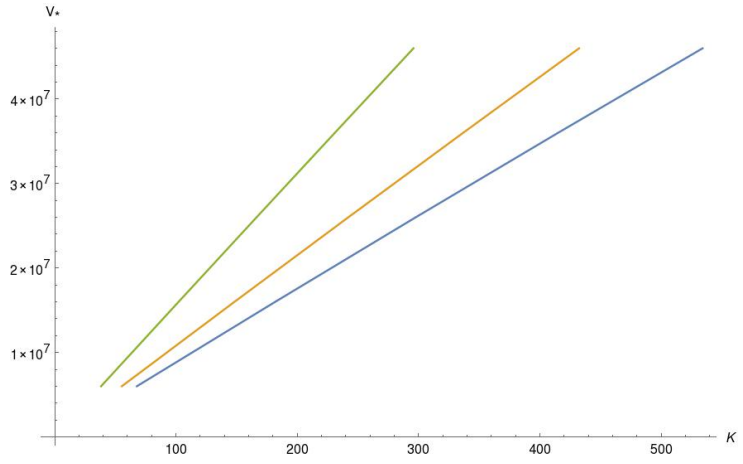

(b)

Figure 3: (a) Example of least squares fitting of the analytical BV model to the tunnelling simulation, red dashed line is the analytical fit and blue dotted line represent the tunnelling simulation. Parameters used: $\alpha = 0.5$, $v* = 1 \times 10^8$ (b) Dimensionlss rate constant and frequency factor relationship fitting for the two models relationship between the two values. Dimensionless Parameters:$R = 1 \times 10^{-4}$, $\beta^* = 8.8 \times 10^4$, 1.1×10^5, 1.57×10^5, $\alpha = 0.5$, $v^* = 1 \times 10^6$ to 4.5×10^7, Equations 28 and 32 were used to calculate the resultant fluxes.

.

Unification of electron tunnelling and the traditional Butler-Volmer Model

The simulation presented above justifies the approach used in previous works,[47] where Butler-Volmer kinetics determines the rate of electron transfer, while the probability of electron transfer is guided by the the exponential fall-off and a frequency factor. As the electron

tunnelling takes place the overall electrical flux is the sum of all contributions from each spatial point and can be represented by an integral defined in Equation 38.

$$f = \int_0^\infty v f_{BV} e^{-\beta x} dx \approx \frac{v f_{BV}}{\beta} \tag{38}$$

β is the decay constant and f_{BV} can be taken as almost constant since the scale of tunnelling is tiny compared to the distance over which the concentration changes in the solution (see below). Accordingly as suggested by Dickinson:[47]

$$v = k_0 \beta \tag{39}$$

Results and Discussion

In this section we first report the concentration profiles obtained for the uniform and near-wall hindered diffusion, obtained through the solution of Equations 32-33. We then investigate the spatially distributed tunnelling current contributions for the two cases. Last the effect of the rotation rate on the resultant limiting current is taken into account and shown in terms of modified "Levich plots". The significant differences for the two cases reflect a significant reduction in the current response for the case of near-wall hindered diffusion.

Concentration Profiles

It is insightful to compare **simulated** concentration profiles obtained for a range of overpotentials for the uniform diffusion case and for the near-wall hindered diffusion in order to develop an understanding of the underlying physical processes. Figure 5 shows the contrasting concentration profile obtained for the two cases. It can be clearly observed that near-wall hindered diffusion (Figure 4b) leads to a lower depletion of the species within close proximity to the electrode in contrast to the uniform case (Figure 4a). The reduced depletion is caused by the reduction in the diffusion coefficient caused by the presence of the solid boundary.

The insets on both graphs show that the boundary condition (Equation 31) is satisfied for both cases within close proximity to the electrode.

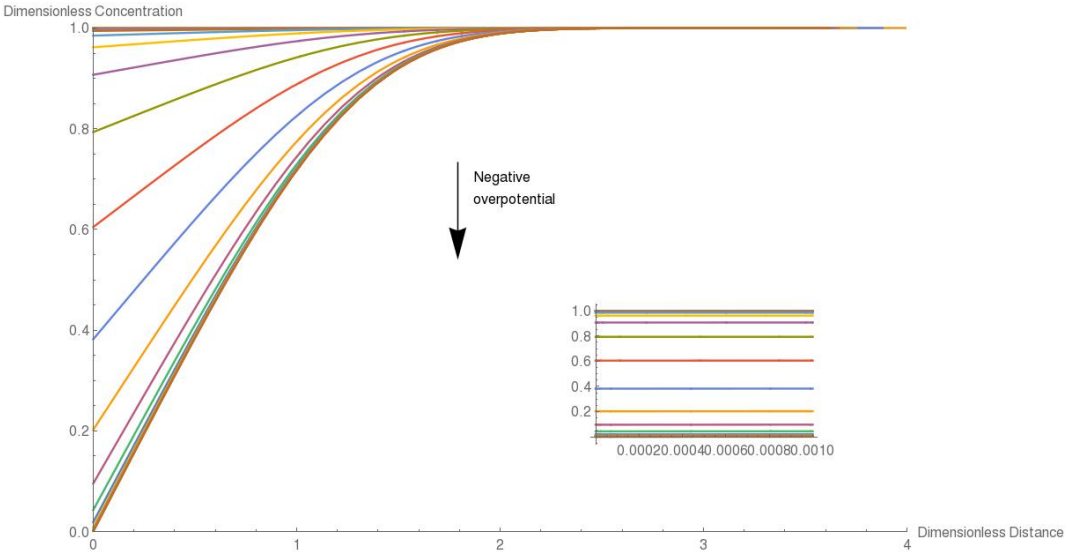

(a)

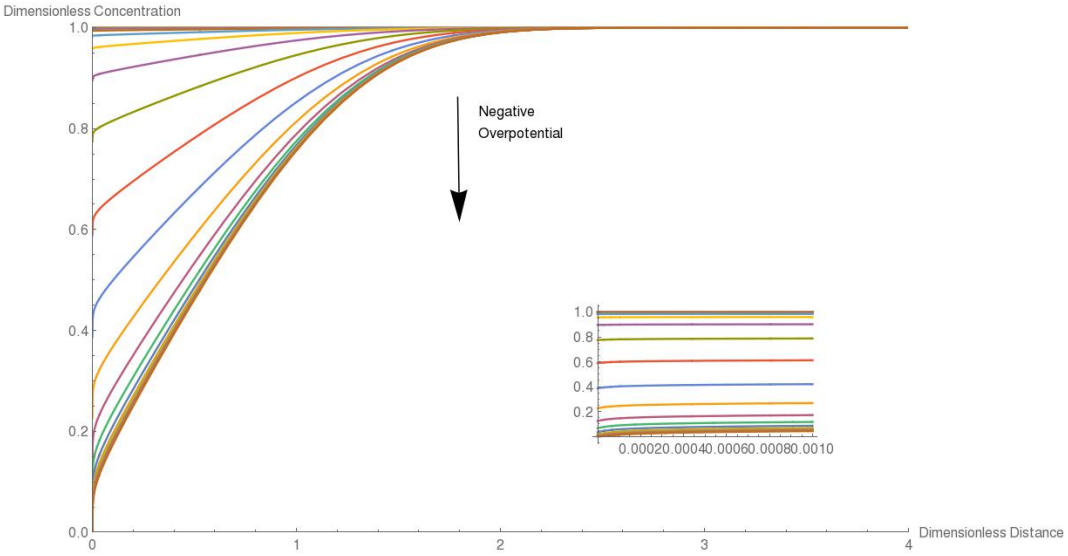

(b)

Figure 4: (a) Uniform diffusion concentration profile for dimensionless potentials -15 to +10, inset shows region within close proximity of the electrode (b) Near-wall hindrance concentration profile for overpotentials -15 to +10, inset shows region within close proximity of the electrode. Dimensionless Parameters: $R = 1.86 \times 10^{-2}$, $\alpha = 0.5$, $v* = 2.3 \times 10^{7}$, $\beta^* = 0.42 \times 10^{5}$. Equations 32 and 33 were used to calculate the resultant concentration profiles.

Figure 5 shows the differences between the two concentration profiles obtained where

$c_{uniform} - c_{hindered}$, $c_{uniform}$ is the uniform diffusion concentration profile and $c_{hindered}$ is the near wall hindered concentration profile. It can be seen that at high overpotential a depletion is present in close proximity to the electrode with a relatively higher concentration further away due to depletion of the layer.

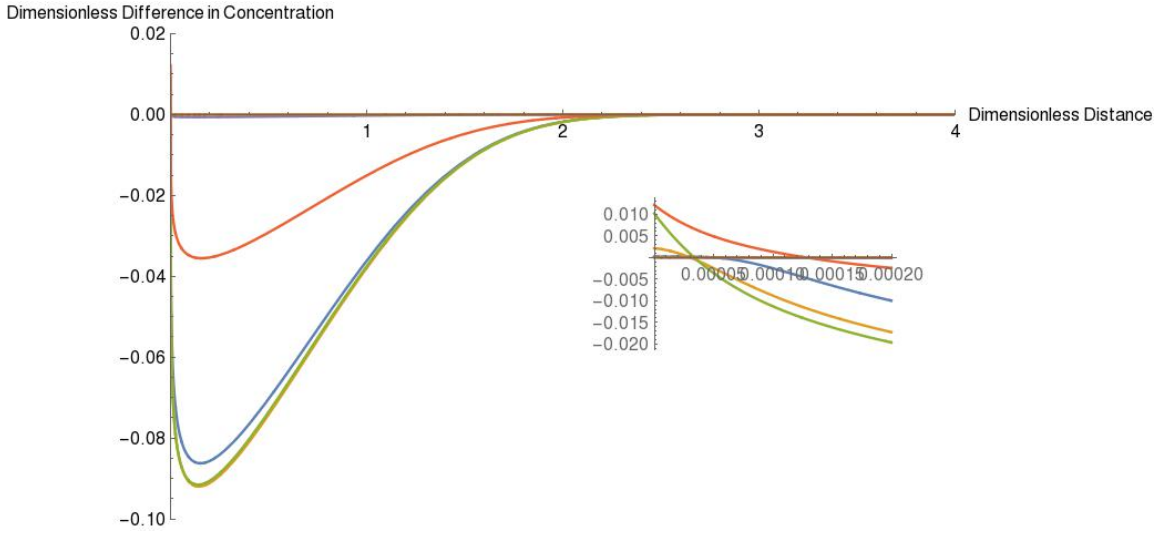

Figure 5: Difference of the concentration profiles obtained for uniform and near-wall hindered diffusion. Dimensionless Parameters: $R = 1.86 \times 10^{-2}$, $\alpha = 0.5$, $v^* = 2.3 \times 10^7$, $\beta^* = 0.42 \times 10^5$. Equations 32 and 33 were used to calculate the resultant concentration profiles and the curves correspond to different potentials.

Flux comparison for the uniform and near-wall hindered diffusion cases

Spatial dependence of the current contribution

Knowledge of the steady-state concentration profile allows the calculation of the current contribution at each point in the solution and is given in accordance with Equation 38. Figure 6 shows the distance-dependent current profile for the species for the uniform (Figure 6a) and near-wall hindered case (Figure 6b). A sharp decay is observed for the case of the uniform diffusion, which is consistent with the sharp decay of tunnelling probability. At high negative overpotentials higher current contribution are observed within close proximity to the electrode. In both cases the electron transfer process is confined to a finite tunnelling

zone and decreases to zero with increasing distance. Surprisingly for the near-wall hindered case a peak appears at high negative overpotentials. Its appearance can be ascribed to the depletion of the species in close proximity to the electrode which results in an overall low contribution to the electrical flux further evidence is the fact that at higher potentials the maximum current contribution shifts further away from the electrode as the depletion layer increases. (Note that this observation might also be attributed to the physical unreality of the Butler-Volmer model at highly negative overpotential: where infinite rates of electron transfer are predicted; for such cases Marcus-Hush theory may be more realistic.)

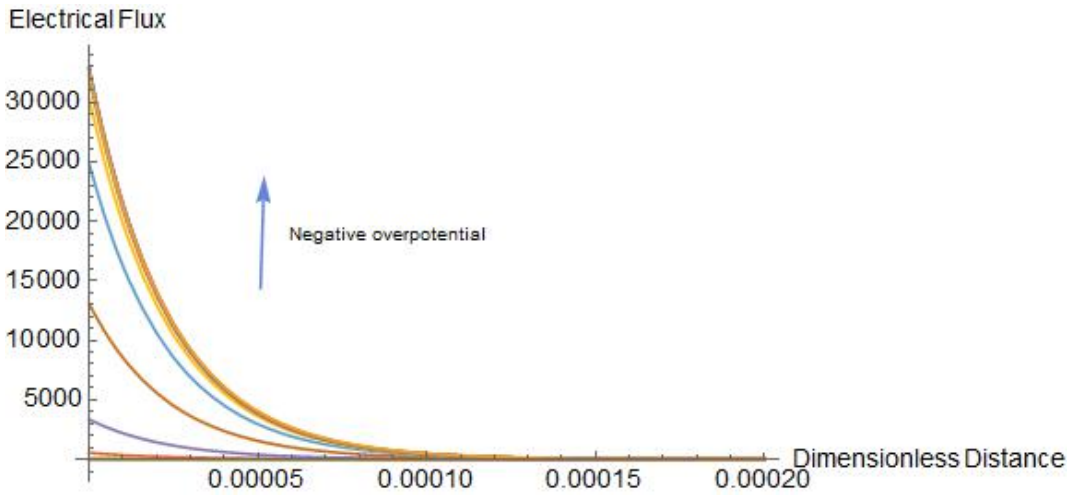

(a)

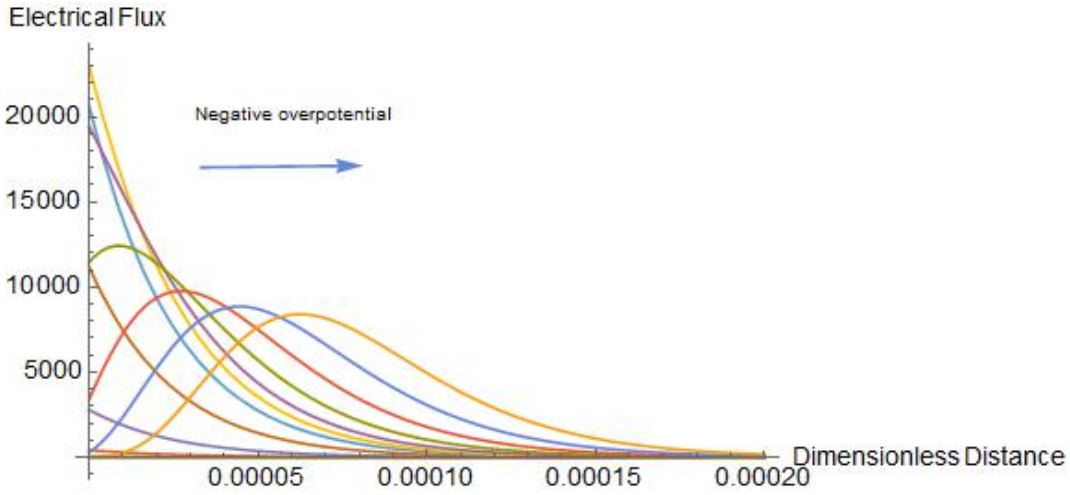

(b)

Figure 6: (a) Uniform spatial electrical flux contribution for overpotentials -15 to +10 (b) Near-wall hindrance electrical flux contribution for overpotentials -15 to +10. Dimensionless Parameters: $R = 1.86 \times 10^{-2}$, $\alpha = 0.5$, $v^* = 2.3 \times 10^7$, $\beta^* = 0.42 \times 10^5$. Equations 32, 33 and 38, were used to calculate the resultant concentration profiles and the curves correspond to different potentials.

Steady state voltammetry response for the uniform and near-wall hindered diffusion

In accordance with the Equation 35 the current output was calculated and the following parameters were used for the conversion to the dimensional form: $A = 7.85 \times 10^{-5}\ m^2$, $c = 1 \times 10^{-3}\ mol\ m^{-3}$. Figure 7 show the steady-state voltammograms in the presence and

absence of the near-wall hindrance. There is a clear difference between the predicted current responses for the two cases. For low positive dimensionless overpotentials ($\approx 2-10$) the effect of near-wall hindrance is not significant due to the fact that the current response is limited kinetically and not by the mass transport of the species. However it can be clearly seen that the effect becomes increasingly important at high overpotentials due to depletion of the diffusion layer at the electrode and significant deviations are observed for large particles.The effect is size-dependent and the discrepancy increases with increasing size of a particle.

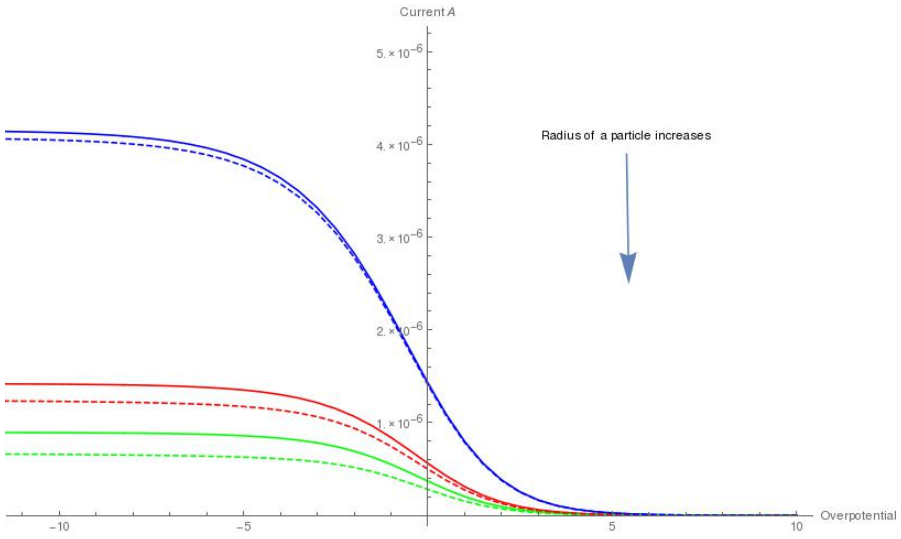

Figure 7: Comparison of linear scan voltammograms for the uniform (solid line) and near-wall hindered (dashed line) cases. The particle radii used in the simulation are 10, 50 and 100 nm respectively. Simulation parameters used $f = 10\ Hz$, $\alpha = 0.5$, $\beta = 1.57 \times 10^{10}\ m^{-1}$, $k_0 = 0.001\ ms^{-1}$, Equations 32 and 33 were used to calculate the resultant concentration profiles.

Effect of the rotation rate on the limiting current response

The rotation speed of the disk has an effect on the thickness of the hydrodynamic layer in accordance with the Equation 1 and as a result at higher rotation rate the limiting current is expected to be proportional to the square root of the rotation rate in accordance with the Equation 8. As a result a linear relationship is expected for the uniform diffusion coefficient but deviations are expected for the case of hindered diffusion. The plot of limiting current against $\sqrt{\omega}$ is known as a 'Levich plot'. Figures 8a-8b shows Levich plots for particle sizes

of 10 and 50 nm. For the 10 nm particle a small deviation is observed at higher rotation but an overall increasing trend is seen as for uniform diffusion. However for the larger 50 nm nanoparticles a significant deviation is observed at higher rotation rates and the plot is non-linear. For the case of 10 nm particle the calculated adjusted R^2 value for linear fit was found to be 0.999875, which is indicative of a closely linear fit. By contrast for the case of 50 nm the calculated adjusted R^2 was 0.996945, which is indicative of the deviation from linearity. As the particle size increases the deviations from linearity increase.

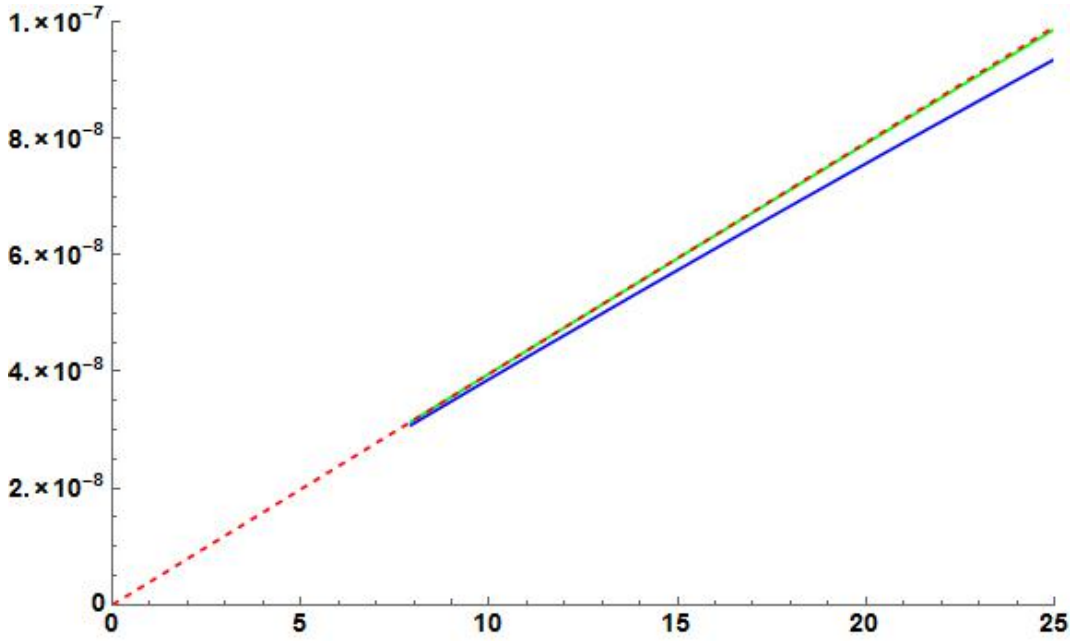

(a)

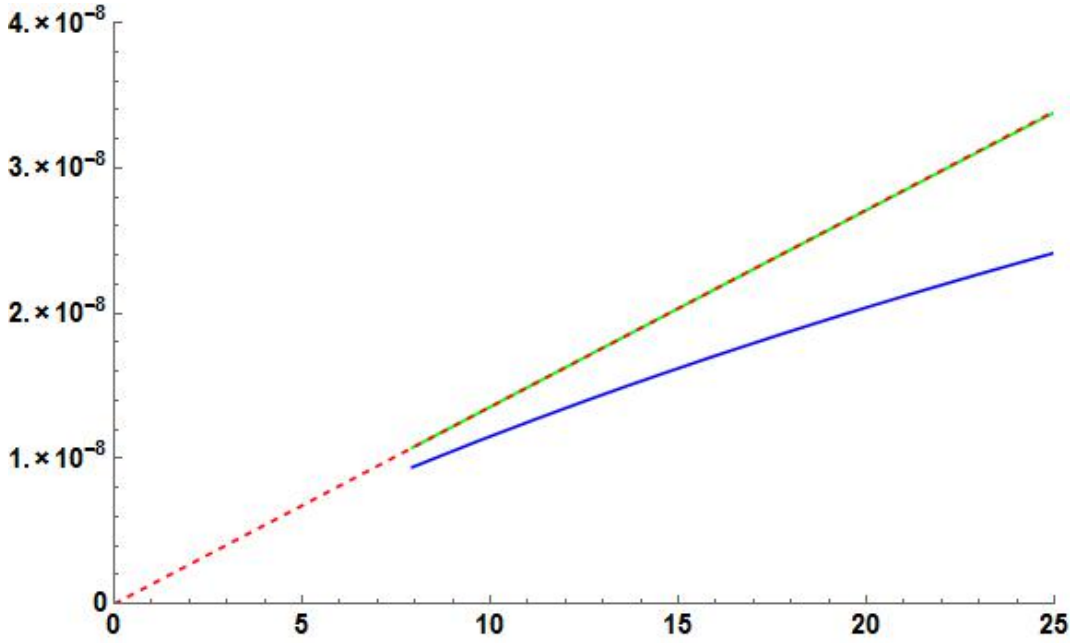

(b)

Figure 8: (a) Levich plots for a particle with a radius of 10 nm: analytical solution (dashed red line), uniform diffusion coefficient with tunnelling (green line) and near-wall hindered diffusion (blue line)(b) Levich plots for a particle with a radius of 50 nm, same color lines were used. Other parameters Simulation parameters used $f = 10\ Hz$, $\alpha = 0.5$, $\beta^* = 1.57 \times 10^{10}\ m^{-1}$, $k_0 = 0.001\ ms^{-1}$, $\eta = 15$. Equations 8, 32 and 33 were used to calculate the electrical flux response.

Conclusions

In the case of convective system a significant impact on mass transport is caused by the near-wall hindrance, the effect is particularly significant for the development of nanoparticle sensors and novel-battery technologies. The near-wall hindrance becomes significant at high overpotentials and high rotation rates and will have a significant effect on applications which rely on these characteristics. Design of the novel nanoparticle sensors and applications such as fuel cells and batteries requires rethinking of the traditional approach to the electrochemical simulations, as approximations valid for molecular are no longer accurate for the case of colloidal suspensions and as a result may lead to a significant error. In addition analysis of the near-wall diffusion hindrance requires the introduction of distance-dependent[58] electron-tunnelling and the traditional measurement of the electrical flux in terms of the concentration gradient at the electrode is invalid.

Supporting Information

The Supporting Information Available:

Figure S1 shows the step-size for the numerical algorithm used for the solution of the differential equations.

Figure S2 shows the Tafel plots for the reversible and irreversible cases.

This material is available free of charge via the Internet at http://pubs.acs.org.

Acknowledgements

We thank Shaltiel Eloul for helpful discussions. The authors declare no conflicting interests. The research leading to these results has received funding from the European Research Council under the European Unions Seventh Framework Programme (FP/2007-2013)/ERC Grant Agreement no.(320403).

References

(1) Beaudin, M.; Zareipour, H.; Schellenberglabe, A.; Rosehart, W. Energy storage for mitigating the variability of renewable electricity sources: An updated review. *Energy Sustain. Dev.* **2010**, *14*, 302–314.

(2) Dincer, I. Renewable energy and sustainable development: a crucial review. *Renew. Sustain. Energy Rev.* **2000**, *4*, 157–175.

(3) Yang, Z.; Zhang, J.; Kintner-Meyer, M. C. W.; Lu, X.; Choi, D.; Lemmon, J. P.; Liu, J. Electrochemical energy storage for green grid. *Chem. Rev.* **2011**, *111*, 3577–613.

(4) Sen, S.; Timofeeva, E. V.; Pelliccione, C. J.; Katsoudas, J. P.; Singh, D.; Segre, C. U. Development of Nanoelectrofuel Electrodes for Flow Batteries : Rheology and Electrochemistry of Fluidized Nanoparticles. *ECS Meet. Abstr.* **2015**, *MA2015-01*, 224.

(5) Sen, S.; Moazzen, E.; Aryal, S.; Segre, C. U.; Timofeeva, E. V. Engineering nanofluid electrodes: controlling rheology and electrochemical activity of γ-Fe2O3 nanoparticles. *J. Nanoparticle Res.* **2015**, *17*, 437–445.

(6) Yao, K.-M.; Habibian, M. T.; O'Melia, C. R. Water and waste water filtration. Concepts and applications. *Environ. Sci. Technol.* **1971**, *5*, 1105–1112.

(7) Molnar, I. L.; Johnson, W. P.; Gerhard, J. I.; Willson, C. S.; O'Carroll, D. M. Predicting colloid transport through saturated porous media: A critical review. *Water Resour. Res.* **2015**, *51*, 6804–6845.

(8) Tian, Y.; Gao, B.; Silvera-Batista, C.; Ziegler, K. J. Transport of engineered nanoparticles in saturated porous media. *J. Nanoparticle Res.* **2010**, *12*, 2371–2380.

(9) Harvey, R. W.; Garabedian, S. P. Use of colloid filtration theory in modeling movement of bacteria through a contaminated sandy aquifer. *Environ. Sci. Technol.* **1991**, *25*, 178–185.

(10) Rajagopalan, R.; Tien, C. Trajectory analysis of deep-bed filtration with the sphere-in-cell porous media model. *AIChE J.* **1976**, *22*, 523–533.

(11) Ma, H.; Johnson, W. P. Colloid retention in porous media of various porosities: predictions by the hemispheres-in-cell model. *Langmuir* **2010**, *26*, 1680–7.

(12) Eral, H. B.; Oh, J. M.; van den Ende, D.; Mugele, F.; Duits, M. H. G. Anisotropic and hindered diffusion of colloidal particles in a closed cylinder. *Langmuir* **2010**, *26*, 16722–9.

(13) Torkzaban, S.; Bradford, S. A.; Walker, S. L. Resolving the coupled effects of hydrodynamics and DLVO forces on colloid attachment in porous media. *Langmuir* **2007**, *23*, 9652–60.

(14) Tufenkji, N.; Elimelech, M. Correlation Equation for Predicting Single-Collector Efficiency in Physicochemical Filtration in Saturated Porous Media. *Environ. Sci. Technol.* **2004**, *38*, 529–536.

(15) Pleskov, Y. V.; Filinovskii, V. Y. *The rotating disk electrode*, 2nd ed.; Consultants Bureau: New York, 1976.

(16) Albery, J. *Electrode Kinetics*; Oxford University Press: Oxford, 1975.

(17) Compton, R. G.; Laing, M. E.; Mason, D.; Northing, R. J.; Unwin, P. R. Rotating Disc Electrodes: The Theory of Chronoamperometry and Its Use in Mechanistic Investigations. *Proc. R. Soc. A Math. Phys. Eng. Sci.* **1988**, *418*, 113–154.

(18) Riese, A.; Banham, D.; Ye, S.; Sun, X. Accelerated Stress Testing by Rotating Disk Electrode for Carbon Corrosion in Fuel Cell Catalyst Supports. *J. Electrochem. Soc.* **2015**, *162*, F783–F788.

(19) Wang, L.; Zhao, X.; Lu, Y.; Xu, M.; Zhang, D.; Ruoff, R. S.; Stevenson, K. J.; Goodenough, J. B. CoMn2O4 Spinel Nanoparticles Grown on Graphene as Bifunctional Catalyst for Lithium-Air Batteries. *J. Electrochem. Soc.* **2011**, *158*, A1379–A1382.

(20) Laoire, C. O.; Mukerjee, S.; Abraham, K. M.; Plichta, E. J.; Hendrickson, M. A. Elucidating the Mechanism of Oxygen Reduction for Lithium-Air Battery Applications. *J. Phys. Chem. C* **2009**, *113*, 20127–20134.

(21) Dolinska, J.; Jonsson-Niedziolka, M.; Sashuk, V.; Opallo, M. The effect of electrocatalytic nanoparticle injection on the electrochemical response at a rotating disc electrode. *Electrochem. commun.* **2013**, *37*, 100–103.

(22) Roberts, J. J. P.; Westgard, J. A.; Cooper, L. M.; Murray, R. W. Solution voltammetry of 4 nm magnetite iron oxide nanoparticles. *J. Am. Chem. Soc.* **2014**, *136*, 10783–9.

(23) Sun, Y.; Dai, Y.; Liu, Y.; Chen, S. A rotating disk electrode study of the particle size effects of Pt for the hydrogen oxidation reaction. *Phys. Chem. Chem. Phys.* **2012**, *14*, 2278.

(24) Kármán, T. V. Über laminare und turbulente Reibung. *ZAMM - J. Appl. Math. Mech. / Zeitschrift für Angew. Math. und Mech.* **1921**, *1*, 233–252.

(25) Cochran, W. The flow due to rotating disk. *Proc. Camb. Philo. Soc.* **1934**, *30*, 365–375.

(26) Incropera, F. P.; DeWitt, D. P.; Bergman, T. L.; Lavine, A. S. *Water*; 2007; Vol. 6th.

(27) Albery, W. J.; Bruckenstein, S. Uniformly accessible electrodes. *J. Electroanal. Chem. Interfacial Electrochem.* **1983**, *144*, 105–112.

(28) Levich, B. The Theory of Concentration Polarization. *Acta Physicochim. U.R.S.S.* **1942**, *17*, 257.

(29) Kuznetsov, A. M.; Petrii, O. A.; Tsirlina, G. A. Veniamin (Benjamin) Grigor'evich Levich (19171987). *Russ. J. Electrochem.* **2008**, *44*, 360–367.

(30) Barnes, E. O.; Zhou, Y.-G.; Rees, N. V.; Compton, R. G. The effect of near wall hindered diffusion on nanoparticleelectrode impacts: A computational model. *J. Electroanal. Chem.* **2013**, *691*, 28–34.

(31) Kätelhön, E.; Compton, R. G. Understanding nano-impacts: impact times and near-wall hindered diffusion. *Chem. Sci.* **2014**, *5*, 4592–4598.

(32) Yoda, M.; Kazoe, Y. Dynamics of suspended colloidal particles near a wall: Implications for interfacial particle velocimetry. *Phys. Fluids* **2011**, *23*, 111301–111309.

(33) Brenner, H. The slow motion of a sphere through a viscous fluid towards a plane surface. *Chem. Eng. Sci.* **1961**, *16*, 242–251.

(34) Kätelhön, E.; Cheng, W.; Batchelor-McAuley, C.; Tschulik, K.; Compton, R. G. Nanoparticle-Impact Experiments are Highly Sensitive to the Presence of Adsorbed Species on Electrode Surfaces. *ChemElectroChem* **2014**, *1*, 1057–1062.

(35) Kihm, K. D.; Banerjee, A.; Choi, C. K.; Takagi, T. Near-wall hindered Brownian diffusion of nanoparticles examined by three-dimensional ratiometric total internal reflection fluorescence microscopy (3-D R-TIRFM). *Exp. Fluids* **2004**, *37*, 811–824.

(36) Pierres, A.; Benoliel, A. M.; Zhu, C.; Bongrand, P. Diffusion of microspheres in shear flow near a wall: use to measure binding rates between attached molecules. *Biophys. J.* **2001**, *81*, 25–42.

(37) Elimelech, M. Particle deposition on ideal collectors from dilute flowing suspensions: Mathematical formulation, numerical solution, and simulations. *Sep. Technol.* **1994**, *4*, 186–212.

(38) Bevan, M. A.; Prieve, D. C. Hindered diffusion of colloidal particles very near to a wall: Revisited. *J. Chem. Phys.* **2000**, *113*, 1228–1236.

(39) Sonneveld, P. J.; Visscher, W.; Barendrecht, E. The influence of suspended particles on the mass transfer at a rotating disc electrode. Non-conducting particles. *J. Appl. Electrochem.* **1990**, *20*, 563–574.

(40) Dabroś, T.; Czarnecki, J. Transport of particles with finite dimensions to a rotating disk surface. *J. Colloid Interface Sci.* **1975**, *53*, 335–336.

(41) Marie de Ficquelmont-Loizos, M. Mass Transfer in Laminar Flow at a Rotating Disk Electrode in Suspensions of Inert Particles. *J. Electrochem. Soc.* **1988**, *135*, 626–634.

(42) Deslouis, C.; Ezzidi, A.; Tribollet, B. Mass transfer enhancement by suspensions in a shear flow. *J. Appl. Electrochem.* **1991**, *21*, 1081–1086.

(43) *Transient Techniques in Electrochemistry*; Springer Science & Business Media, 2012.

(44) Bond, A. M. *Broadening Electrochemical Horizons: Principles and Illustration of Voltammetric and Related Techniques*; Oxford University Press, 2002.

(45) Compton, R. G.; Laborda, E.; Ward, K. R. *Understanding Voltammetry Simulation of Electrode Processes*; Imperial College Press, 2014.

(46) Bard, A.; Faulkner, L. *New York*, 2nd ed.; Wiley: New York, 2001.

(47) Dickinson, E. J.; Compton, R. G. Influence of the diffuse double layer on steady-state voltammetry. *J. Electroanal. Chem.* **2011**, *661*, 198–212.

(48) Gavaghan, D. J.; Feldberg, S. W. Extended electron transfer and the Frumkin correction. *J. Electroanal. Chem.* **2000**, *491*, 103–110.

(49) Marcus, R. A.; Siders, P. Theory of highly exothermic electron transfer reactions. *J. Phys. Chem.* **1982**, *86*, 622–630.

(50) Kätelhön, E.; Compton, R. G. Understanding Nano-Impacts: Binary Nature of Charge Transfer during Mediated Reactions. *ChemElectroChem* **2015**, *2*, 64–67.

(51) Edwards, P. P.; Gray, H. B.; Lodge, M. T. J.; Williams, R. J. P. Electron Transfer and Electronic Conduction through an Intervening Medium. *Angew. Chemie Int. Ed.* **2008**, *47*, 6758–6765.

(52) Hugelmann, M.; Schindler, W. Tunnel barrier height oscillations at the solid/liquid interface. *Surf. Sci.* **2003**, *541*, L643–L648.

(53) Compton, R. G.; Banks, C. E. *Understanding Voltammetry*, 2nd ed.; Imperial College Press, 2010.

(54) Guidelli, R.; Compton, R. G.; Feliu, J. M.; Gileadi, E.; Lipkowski, J.; Schmickler, W.; Trasatti, S. Defining the transfer coefficient in electrochemistry: An assessment (IUPAC Technical Report). *Pure Appl. Chem.* **2014**, *86*, 245–258.

(55) Guidelli, R.; Compton, R. G.; Feliu, J. M.; Gileadi, E.; Lipkowski, J.; Schmickler, W.; Trasatti, S. Definition of the transfer coefficient in electrochemistry (IUPAC Recommendations 2014). *Pure Appl. Chem.* **2014**, *86*, 259–262.

(56) Feldberg, S. W. Implications of extended heterogeneous electron transfer. *J. Electroanal. Chem. Interfacial Electrochem.* **1986**, *198*, 1–18.

(57) Teukolsky, S.; Vetterling, W.; Flannery, B. *Cambridge Univ. Press*; 2007.

(58) Bartlett, T. R.; Sokolov, S. V.; Compton, R. G. Electrochemical Nanoparticle Sizing Via Nano-Impacts: How Large a Nanoparticle Can be Measured? *ChemistryOpen* **2015**, *4*, 600–605.

Graphical TOC Entry